Platinum-zeolite hybrid catalyst for the electrooxidation of formic acid

Lu Zhang, Juan Perales-Rondón, Angélica Thomère, Juliette Blanchard, Carlos Sánchez-Sánchez

Platinum-zeolite hybrid catalyst for the electrooxidation of formic acid

Lu Zhang[a,b], *Juan V. Perales-Rondón*[a,c], *Angélica Thomère*[a,b], *Juliette Blanchard*[b], *Carlos M. Sánchez-Sánchez**[,a],

[a]*Sorbonne Université, CNRS, Laboratoire Interfaces et Systèmes Electrochimiques, 4 place Jussieu, F-75005 Paris, France*

[b]*Sorbonne Université, CNRS, Laboratoire de Réactivité de Surface, LRS UMR 7197, F-75005, Paris, France.*

[c]*Instituto Universitario de Electroquímica, Universidad de Alicante, Ap. 99, 03080, Alicante, Spain*

Abstract

Formic acid oxidation reaction (FAOR) was studied using different platinum-zeolites hybrid catalysts. The catalysts were prepared by addition of two different forms of the ZSM-5 zeolite (ZSM-5-H^+ and ZSM-5-NH_4^+) to an ink containing Vulcan carbon support and Pt nanoparticles (NPs). TEM images demonstrate a proper mixture of the components in the ink and a good dispersion of the Pt NPs mainly over the carbon. Both zeolites (ZSM-5-NH_4^+ and ZSM-5-H^+) are stable under electrochemical conditions for FAOR, but ZSM-5-NH_4^+ undergoes fast conversion into ZSM-5-H^+ due to the exchange between the compensator cation in the zeolite and protons in solution.

A significant enhancement on the catalytic activity was found for both zeolite hybrid catalysts, being the ink containing ZSM-5-H^+ the more stable over time. In particular, 7

and 10 times larger current densities than on 9 wt.% Pt/C were achieved by the (7 wt.% Pt/18.5 wt.% ZSM-5-NH_4^+/C) and the (7 wt.% Pt/18.5 wt.% ZSM-5-H^+/C) catalysts in chronoamperometry, respectively. The results demonstrated the beneficial and synergetic effect of the addition of zeolites in order to improve the catalytic activity of Pt NPs. The addition of zeolite ZSM-5 within the electrocatalyst did not provoke any relevant modification in the type of features displayed in cyclic voltammetry, but provoked a significant enhancement of the peak current density associated with the CO stripping. We propose that the mechanism for this improvement lies in a more efficient distribution of Pt nanoparticles on the catalytic ink thanks to the presence of zeolites and the preconcentration of the reactant (HCOOH) within the zeolite microporosity occurring in solution. Moreover, local pH modifications associated with the NH_4^+/H^+ exchange could have some impact on the kinetics of the FAOR by the *direct via*.

Keywords

Hybrid catalyst; zeolites; preconcentration; Formic acid oxidation; Pt nanoparticles.

1. Introduction

Nowadays a lot of effort is concentrated on developing large scale electrochemical systems for formic acid (HCOOH) production as an efficient and feasible method to recycle CO_2 from the atmosphere [1-3]. In the same context, electrooxidation of formic acid represents a relevant reaction to recover the electrical energy stocked in that molecule and direct formic acid fuel cells (DFAFCs) have been proposed to be used as small power suppliers in electronic devices [4-6]. As a fuel, formic acid presents fast oxidation kinetics, less fuel crossover through the ion exchange membrane compared with other fuels such as methanol, and is also easy to handle and manipulate once produced. Additionally,

formic acid oxidation reaction (FAOR) is one of the most studied reactions in electrocatalysis, since it can be used as a model in fundamental studies of reaction mechanism for small organic molecules (SOM) [7]. More specifically, formic acid oxidation on platinum electrodes has been widely studied over the last two decades [8], because of the high activity of this metal for the oxidation of organic molecules. Furthermore, the comprehension of the reaction mechanism on this metal can be extrapolated to other important metallic catalysts.

It is well known in the literature that formic acid oxidation on platinum electrodes presents two different reaction pathways [9-11]. The first one is the so-called *indirect via*, which involves the initial formation of adsorbed CO that acts as a poison intermediate followed by its subsequent oxidation to CO_2 at higher overpotential values. The second pathway is known as the *direct via*, and implies the formation of an active intermediate, which is immediately oxidized into CO_2 at lower overpotential values.

Different methods have been used to improve the performance of Pt catalysts to FAOR. One of them is based on increasing the amount of highly active specific crystallographic sites on the electrode surface by controlling size and/or shape of nanoparticles (NPs) [12,13]. Another method to enhance Pt specific activity is to modify the chemical composition of the Pt catalyst by either forming an alloy with other d-band metals such as Pd, Au or Ru [14,15] or adding a foreign adatom such as Bi, Sb or Pb [16-18], which might be adsorbed and deposited as a sub-monolayer. In both cases, a relevant effect on the FAOR mechanism is produced by strongly supressing the CO formation and/or promoting the FAOR by the direct via [19,20].

Zeolites are very useful materials in heterogeneous catalysis, but have been mainly used at the solid/gas interface. Zeolites are microporous crystalline aluminosilicates

(SiO_2/Al_2O_3) that provides a high surface area and molecular-sized cavities (cavities with sizes in the range 0.3-1.2 nm). The zeolite pore dimension allows physical exclusion or inclusion of specific molecules or ions. In fact, size exclusion plays a major role in adsorption of molecules within the microporosity of zeolites. A few examples have been already reported in the literature taking advantage of this physical exclusion property in electrocatalysis. For instance, different thin films of Na zeolite A (4 Å pore size) and K zeolite A (3 Å pore size) have been synthesized on conducting SnO_2 electrodes for behaving as a nanoporous filter in an electrochemical environment [21]. The Na zeolite A film let pass specific molecules such as molecular oxygen (3.145 Å molecular dimeter) to the electrode surface and simultaneously reject larger diameter interference species by size exclusion. Nevertheless, the diffusion coefficient of oxygen gets reduced by two orders of magnitude within the zeolite pores, which reduces the limiting current for oxygen reduction reaction that can be achieved. A similar approach has been also explored on mesoporous (2-3 nm in diameter) silica films grown on electrodes [22-24]. In addition to the sub-nanometer filters application, zeolites modified with redox-active guests [25] and zeolite particles mixed together with the catalyst for the electrochemical oxidation of small organic molecules [26-34] have also exhibited interesting results in different electrochemical systems. Different types of zeolites have been used as support for metallic nanoparticles in widely studied electrocatalytic reactions such as methanol [26-28] and formaldehyde oxidation reactions [32]. In most cases, zeolites have a positive impact on the electrochemical activity (by decreasing the onset potential and increasing the oxidation current) [28]. Several possible causes have been already proposed in the literature for explaining this activity enhancement: a lower ohmic drop (thanks to the hydrophilic nature of zeolites), a higher tolerance of Pt NPs to CO (because of a modification of the electronic density of Pt NPs by the zeolite), a higher dispersion of

platinum, an enhanced capability of the Pt NPs to oxidize CO (thanks to the oxygen-rich environment of zeolites) [28, 32]. Nevertheless, the electroactive species preconcentration within the zeolite microporosity was never proposed before, although the adsorption of small organic molecules, such as alcohols and carboxylic acids, from diluted aqueous solutions within the porosity of zeolites (including zeolite Socony Mobil-5 (ZSM-5)) is well established [35-40]. Moreover, several authors has proposed zeolite adsorption as an efficient separation method for recovering those organic molecules from aqueous effluents [38].

A conventional approach to improve the sensitivity in electroanalysis of trace metals is the analyte preconcentration [41]. Preconcentration electroanalysis of paraquat, a pesticide, by electrostatic binding to mesoporous silica has been previously reported [42] and zeolites have been already used for ex-situ preconcentration by solid phase extraction [43], but never for in-situ preconcentration, which is the main goal of the present work.

Exploring the adsorption in zeolites at the solid-liquid interface requires to take into consideration the hydrophilicity/hydrophobicity of zeolites, which is governed by the Si/Al ratio. For electrochemical applications in aqueous solutions, only zeolites such as faujasite, ZSM-5 and beta, with moderately high Si/Al ratio (hydrophilic zeolites, Si/Al<40), can be envisaged, because strongly hydrophobic zeolites present almost zero water adsorption capacity making them poorly efficient in electrochemical conditions. In these hydrophilic zeolites, solute and solvent molecules may compete for the adsorption sites within the micropores, as has been already demonstrated for ethanol and acetic acid aqueous solutions adsorbed on ZSM-5 [37]. However, the adsorption within the zeolite is not only controlled by the molecule size, but also by the affinity of the solute for the solvent vs. the zeolite cavities. Experimental isotherms can be fitted using different adsorption models depending on the type of organic molecule in solution [39]. In

particular, high silica zeolites such as ZSM-5 have been shown to be effective for the adsorption of formic and/or acetic acids [35, 37-38, 40]. Adsorption isotherms for formic acid aqueous solutions have been already reported in the beta zeolite (SiO_2/Al_2O_3 = 18) and co-adsorption of formic acid and water following the isotherm type Freundlich has been established [40].

Despite the fact that zeolites are insulator materials, hydrated zeolites present an inter- and intra-crystallite cationic conduction, because they behave as an electrolyte, thanks to the water adsorbed in their cavities [25, 44]. Additionally, the presence of metallic nanoparticles in their pores can also increase their conductivity by several orders of magnitude [45]. With this picture in mind, the objective of the present work is to show the potential of local preconcentration of electroactive species (formic acid, molecular diameter 3.81 Å) within the electrode interface using zeolite ZSM-5 (channel diameter 5-6 Å) as one of the components within the catalytic ink forming the (Pt/ZSM-5/Carbon) hybrid catalyst for FAOR in acidic media and to establish the feasibility of using such materials for conferring higher catalytic activity and stability to real DFAFCs.

2. Material and methods

2.1.Preparation of the electrocatalytic ink

Commercial colloidal Pt spherical nanoparticles (0.05 mg Pt/mL) with average size of 4 nm were supplied by Metrohm-DropSens. Commercial zeolite ZSM-5-NH_4^+ (specific surface = 425 $m^2 \cdot g^{-1}$, particle size distribution < 4.2 µm), (SiO_2:Al_2O_3 = 28:1) was supplied by Alfa-Aesar. Zeolite ZSM-5-H^+ was obtained after calcination of ZSM-5-NH_4^+ in a muffle furnace for 5h at 500ºC in air (SiO_2:Al_2O_3 = 28:1). A size selection on zeolite particles was operated in order to obtain suspensions of zeolite particles with a

reasonable stability over time (stability of ca. 1h) and to ensure a good contact between the components of the hybrid electrode. This size selection was achieved by selectively removing larger particles (size >1 μm) from an isopropanol/zeolite suspension using centrifugation at 1500 rpm. SEM micrographs of size-selected ZSM-5-NH_4^+ and ZSM-5-H^+ are shown in Figure 1. Commercially available carbon Vulcan XC-72R, a conductive carbon black from Cabot Co. with an average particle size of 50 nm (see Figure 1), was used as carbon support. Nafion solution 5% w/w in a mixture of lower aliphatic alcohols and water was employed as ionic conductor.

The colloidal suspension of platinum NPs, carbon and ethanol were mixed together and sonicated for 90 min. The isopropanol suspension containing the zeolite ZSM-5 particles was pretreated with ultrasound for 10 minutes and then added to the previous suspension. The resulting suspension was treated with ultrasound for half an hour before addition of diluted Nafion solution (1:9 v/v in ethanol). The final suspension (electrocatalytic ink) was treated with ultrasound for another 15 minutes before dropping 4 μL on a glassy carbon disc electrode (diameter = 3 mm) used as current collector and dried for 30 min. Several ink compositions were evaluated herein: (9 wt.% Pt/C), (7 wt.% Pt/10 wt.% ZSM-5-NH_4^+/C), (7 wt.% Pt/18.5 wt.% ZSM-5-NH_4^+/C), (7 wt.% Pt/25 wt.% ZSM-5-NH_4^+/C) and (7 wt.% Pt/18.5 wt.% ZSM-5-H^+/C).

2.2.Zeolites stability tests in acid solution

In order to investigate the chemical and structural stability of the zeolite ZSM-5 immersed in acid aqueous solution under electrocatalytic conditions, 1g of zeolite (either ZSM-5-NH_4^+ or ZSM-5-H^+) was suspended in a 0.5 M H_2SO_4 solution and the suspension was stirred during 24h. The solid phase was recovered by centrifugation, washed 3 times

with distilled water and dried in the oven at 50°C during 1 night before evaluating the effect of that treatment on the zeolite crystallinity and amount of acid catalytic sites.

2.3.Physicochemical characterization

Crystallinity of zeolites was investigated using X-ray diffraction (XRD) with a Bruker D8 ADVANCE diffractometer (Cu Kα radiation) over a 2θ range from 5° to 80° with a step size of 0.02° and a counting time of 0.5 s per step. Chemical composition of zeolites (ratio SiO_2/Al_2O_3) was determined using X-ray fluorescence (XRF) analysis; experiments were conducted under He flow with an energy dispersive spectrometer (XEPOS with Turboquant powder software) equipped with a 50-Watt end-window X-ray tube. In addition to this, the extent of NH_4^+/H^+ exchange between the compensator cation in the zeolite ZSM-5-NH_4^+ and the protons in solution was estimated based on thermodesorption experiments followed by mass spectrometer. About 0.3 g of zeolite ZSM-5-NH_4^+ were heated under He flow (25 ml min^{-1}) from RT to 700°C. NH_3-desorption was monitored by following m/z=15 -corresponding to NH- and the amount of desorb NH_3 was estimated by integrating the desorption peak and using a calibration curve performed by injecting NH_3 pulses of known volume.

The morphology and size of the zeolites and carbon Vulcan XC-72R were characterized using scanning electron microscopy (SEM) (Zeiss, Supra 55 microscope). Moreover, transmission electron microscopy (TEM) measurements were performed to estimate both particle size and distribution of all 3 components present in the electrocatalytic ink. Experiments were performed using a JEOL 2010 microscope operating at 200 kV with a LaB_6 filament and equipped with an Orius CCD camera (Gatan).

2.4.Electrochemical characterization

Cyclic voltammetry (CV) and chronoamperometry (CA) were performed using a conventional electrochemical glass cell of 3 electrodes at room temperature and a potentiostat (either CHI 760E or CHI 920D). The working electrode was prepared by drop casting 4 µL of each electrocatalytic ink on a 3 mm diameter glassy carbon disc electrode. A platinum wire (d = 0.5 mm) was used as a counter electrode, and Hg/Hg_2SO_4 within a Luggin capillary was employed as a reference electrode. All potentials used in this work were converted to *RHE* ($E_{Hg/Hg2SO4}$ = +0.64 V vs RHE).

CVs for evaluating the electrochemical surface area (ECSA) of Pt in the different electrocatalytic inks were carried out in a 0.5 M H_2SO_4 (Sigma-Aldrich TraceSELECT 95%) solution deaerated with Ar (N60, Air Liquide). The ECSA value was determined by quantifying the charge involved in the voltammetric peaks corresponding to the hydrogen desorption within the hydrogen underpotential deposition region (between 0.05 and 0.35 V/RHE) after subtraction of the double layer contribution [46]. 210 µC cm^{-2} was adopted as the calibration charge density for desorption of a complete monolayer of H atoms on polyoriented Pt electrodes [47]. CVs and CAs for studying the electrocatalytic activity for FAOR were carried out in deaerated 0.1 M HCOOH (Merck KGaG 98 %) and 0.5 M H_2SO_4 solution. An electrochemical pre-treatment for removing the CO_{ads} accumulated at the electrode surface from previous FAOR experiments was performed before starting each CA. This consists in holding the electrode potential at 0.95 V vs RHE for 5 s.

3. Results and discussion

ZSM-5 zeolite immersed in solution under electrochemical conditions for performing FAOR may undergo numerous modifications. Indeed, the acid pH solution used for the reaction may provoke several effects: (i) zeolite may not be fully stable in these conditions and an amorphous phase could be developed; (ii) extraction of framework aluminum could occur, leading to a decrease in the number of acid sites; (iii) for the ammonium form of the zeolite, NH_4^+ cations may be ion exchanged by the protons in solution. In order to investigate all these potential modifications, zeolite samples have been aged under electrochemical conditions and characterized in terms of stability /amorphisation (XRD), extraction of aluminum atoms (XRF) and NH_4^+ content (thermal desorption of NH_3).

The X-ray diffractograms of the fresh and aged ZSM-5 zeolites are shown in Figure 2. All four diffractograms are identical and no amorphous phase is detected. This indicates that neither the calcination step (used to convert ZSM-5-NH_4^+ into ZSM-5-H^+) nor the aging in acidic solution (24 h immersion in 0.5 M H_2SO_4 solution) induces a detectable amorphisation of the zeolite. X-ray fluorescence analysis proves that the two fresh zeolites have the same chemical composition (SiO_2:Al_2O_3 = 28:1) and the composition of the two zeolites are only very marginally modified after a prolonged aging in acidic solution (SiO_2:Al_2O_3 = 30:1), indicating that a very small fraction of Al atoms are extracted from the zeolite framework. Moreover, for the ZSM-5-NH_4^+ case, the aged zeolite was further compared to the starting zeolite in order to evaluate the extent of H^+/NH_4^+ exchange produced in acidic solution. NH_4^+ titration by thermodesorption indicates that about 84% of NH_4^+ are ion-exchanged by protons after immersion in acidic solution for 2h. Thus, both zeolites (ZSM-5-NH_4^+ and ZSM-5-H^+) are stable under

electrochemical conditions for FAOR, but ZSM-5-NH_4^+ undergoes fast conversion into ZSM-5-H^+ due to the exchange between the compensator cation in the zeolite and protons in solution.

The addition of ZSM-5 zeolites could provide a synergetic effect in the catalytic activity of conventional Pt/C catalysts for FAOR. With the aim of demonstrating such a statement, a systematic study of FAOR activity of different Pt electrocatalytic inks was performed. Figure 3 shows the TEM micrographs of two different hybrid catalytic inks studied in this work, prepared adding Pt NPs, carbon support (Vulcan XC-72R) and either ZSM-5-H^+ (Figure 3a) or ZSM-5-NH_4^+ (Figure 3b) zeolites. On both images, one clearly observes that Pt NPs are supported on the carbon particles. This was expected considering that the size of the Pt NPs (4 nm) does not allow them to enter the zeolite micropores (5 Å). One can also observe that carbon particles are well interconnected with the zeolites. Moreover, TEM images show a good dispersion of the Pt NPs on the carbon support. This structure ensures an ideal access of both reactant and electrolyte to the Pt electrocatalyst.

Figure 4a shows the conventional cyclic voltammetry for FAOR on Pt NPs supported on carbon (blue plot) compared with the blank in the absence of HCOOH in solution (black plot). This type of voltammogram has been extensively described in the literature [48], since Pt exhibits common electrochemical features oxidizing different small organic molecules [49]. The main features within the positive-going sweep (blue solid line in Figure 4a) correspond to the so-called *indirect via*, which involves the formation of adsorbed CO from HCOOH dehydration that poisons the metallic sites. The onset of the oxidation peak centred at 0.85 V vs RHE corresponds to the start of the stripping of CO_{ads} by OH_{ads}, which becomes the rate determining step of the FAOR. Higher potential values than the CO stripping peak provoke the increased coverage of Pt surface by adsorbed OH and subsequent Pt surface oxidation. In contrast, the main feature

on the negative-going sweep (blue dashed line in Figure 4a) corresponds to a high activity oxidation peak centred at 0.5 V vs RHE, which can be assigned to the FAOR by the *direct via*, coupled to the reduction of the Pt oxide (peak centred at 0.65 V vs RHE and shown in the black plot in Figure 4a) previously formed during the positive-going sweep.

The addition of zeolite ZSM-5 within the electrocatalyst allows a higher dispersion of Pt NPs, which is demonstrated by comparing ECSA values calculated from the cyclic voltammograms in the absence of HCOOH in solution (black plots in Figure 4). ECSA values for Pt-zeolite hybrid catalysts are 3 times larger than for Pt/C. However, this difference is already taken into account when comparing the FAOR activity displayed by those catalysts in Figure 4, since specific current density is reported. Figures 4b and c display the cyclic voltammetry for FAOR corresponding to two different Pt-zeolites hybrid catalysts. The addition of ZSM-5 does not provoke any relevant modification in the type of features displayed by the CV, but provokes a significant enhancement of the peak current density associated with the CO stripping at 0.85 V (figures 4b and c) in comparison with the one displayed by Pt/C (figure 4a). Moreover, in the ZSM-5-NH_4^+ case, a significant enhancement of FAOR by the *direct via* is also observed on the negative-going sweep (figure 4b). This behaviour can be explained by the exchange between the compensator cation in the zeolite ZSM-5-NH_4^+ and protons in solution, which does not happen when ZSM-5-H^+ participates in the hybrid electrocatalyst. As has been stated in the literature, FAOR is highly dependent on solution pH [50-51]. Hence, local pH modifications due to the NH_4^+/H^+ exchange could have some impact on the kinetics of the FAOR by the *direct via*.

The oxidation current density enhancement associated with the CO stripping at 0.85 V displayed by the Pt-zeolites hybrid catalysts, which cannot be associated with a change in the reaction mechanism, is compatible with a higher local concentration of HCOOH

within the diffusion layer of the electrode due to the release of HCOOH previously preconcentrated within the microporosity of ZSM-5. This preconcentration step most likely happens within the time gap devoted to deoxygenation of the solution by argon bubbling before starting the electrochemical measurements on the electrocatalyst, but continues meanwhile the electrode is immersed in solution, since zeolite particles are continuously exposed to 0.1 M HCOOH in solution. Moreover, several previous works have demonstrated that Pt catalysts supported on zeolite present a major tolerance to the CO formation on the catalyst surface, due to the intrinsic capability of zeolites to facilitate CO reaction with OH groups [25, 30-31].

The percentage of zeolite in the electrodes characterized by cyclic voltammetry on Figure 4b and c was 18.5 wt.%. This zeolite loading was selected after testing different catalysts prepared with different amounts of zeolite. Figure 5 shows the overlay of cyclic voltammograms for FAOR of 3 different hybrid catalysts containing 10, 18.5 and 25 wt. % of ZSM-5-NH_4^+ in their composition. Figure 5 shows that 18.5 wt. % of zeolite corresponds to an optimum loading in terms of HCOOH oxidation current density by the direct via and at the CO stripping peak at ca. 0.85 V. The decrease in current observed at higher percentage of zeolites (25 wt. %) can be assigned to an increase in the ohmic drop within the hybrid catalyst due to the insulator nature of zeolites. In contrast, the decrease in current observed at low zeolite loading (10 wt. %) indicates that the zeolite content is too low to improve significantly the catalytic activity.

One way to evaluate the stability of an electrocatalyst is to perform chronoamperometries at specific potentials. Figure 6 shows the chronoamperometric curves at two different applied potentials (0.54 and 0.74 V vs RHE) for conventional Pt/C catalyst and the two Pt-zeolite hybrid catalysts (9 wt.% Pt/C, 7 wt.% Pt/18.5 wt.% ZSM-5-NH_4^+/C and 7 wt.% Pt/18.5 wt.% ZSM-5-H^+/C). As can be expected, for the three

samples, the current densities are larger at 0.54 V than at 0.74 V and undergo slow decrease over time following Cotrell equation, as expected for a macroelectrode. After 200 s a pseudo-steady state is reached for all samples. Moreover, the two Pt-zeolite hybrid catalysts produce a significantly higher current density than the Pt/C catalyst. In particular, 7 and 10 times larger current densities at pseudo steady-state are achieved by the 7 wt.% Pt/18.5 wt.% ZSM-5-NH_4^+/C and the 7 wt.% Pt/18.5 wt.% ZSM-5-H^+/C catalysts, respectively. When comparing the behaviour of the two Pt-zeolite hybrid catalysts, it is clear that, although ZSM-5-NH_4^+ (red plot in Figure 6) present higher initial current densities, the hybrid catalyst containing ZSM-5-H^+ (green plot in Figure 6) displays a more stable activity for FAOR, since the rate at which the current density decreases is slower than in the case of ZSM-5-NH_4^+. This fact is probably due to the local pH modification associated with the exchange between the compensator cation in the zeolite ZSM-5-NH_4^+ and protons in solution.

The results shown in Figures 4 and 6 evidence that the incorporation of ZSM-5 as a part of the electrocatalyst improves the catalytic activity of Pt NPs for FAOR when compared with a conventional Pt-NPs/C electrocatalyst. Enhancement of the catalytic activity for the oxidation of different small organic molecules on Pt NPs-based electrodes upon addition of zeolite has already been previously observed. However, in most of the previous studies, Pt NPs where located within the zeolite porosity. This is however not the case in the present study as the size of the preformed Pt NPs used for the preparation of the electrocatalyst (about 4 nm) does not allow them to enter the pores of ZSM-5 (ca 5 Å). This affirmation is confirmed by the TEM micrographs of the corresponding inks (Figure 3) that clearly establish that the Pt NPs are located on the carbon particles. Hence, some of the hypotheses initially listed regarding the promoting role of zeolite should be reconsidered. For example, one can exclude a modification of the electronic properties of

the Pt NPs by the presence of zeolite particles in the hybrid catalyst. However, a more efficient distribution of Pt NPs on the hybrid catalysts have been confirmed in this work. Thus, we propose an additional hypothesis based on the excellent adsorption properties of high silica zeolites for formic or acetic acids in aqueous solution, which are well documented in the literature [35, 37-38, 40]. In principle, either reactant (HCOOH) preconcentration or products (CO_2) adsorption within the microporosity of ZSM-5 can contribute to justify the significant current density enhancement observed in hybrid catalysts by cyclic voltammetry and chronoamperometry. In both cases, diffusion of species is necessary, either HCOOH diffusion from the zeolite microporosity to the solution in the vicinity of Pt NPs or CO_2 diffusion from the Pt surface towards the zeolite. Nevertheless, the concentration gradient established by the HCOOH consumption within the diffusion layer of the hybrid electrode drives HCOOH out of the zeolite, which is not the case for CO_2, since the concentration gradient drives CO_2 into the bulk solution. For this reason, we propose a continuous local preconcentration of HCOOH (molecular diameter 3.81 Å) within ZSM-5 (microporosity size 5-6 Å) as one of the dominant effects enhancing catalytic activity reported here for FAOR on hybrid Pt-zeolite catalysts.

4. Conclusions

We present here platinum-zeolites hybrid catalysts prepared using two different zeolites (ZSM-5-H^+ and ZSM-5-NH_4^+) and three different loading of ZSM-5 (10, 18.5 and 25 wt. %). The characterization of the hybrid catalysts showed a good homogeneity of the composites (good distribution of ZSM-5 and carbon Vulcan NPs), Pt NPs essentially located on the carbon support and a more efficient dispersion of the Pt NPs in comparison with Pt/C. The stability tests performed on the ZSM-5 particles immersed in solution under electrochemical conditions indicated a good stability of the zeolite particles

(absence of amorphisation and moderate extraction of framework aluminium atoms). This conclusion is supported by comparing XRD, XRF and NH_3 thermodesorption data performed on fresh and aged samples. The presence of zeolites improves not only the catalytic activity, but also the stability of both hybrid catalysts, being that containing ZSM-5-H^+ the more stable on time, as demonstrated by chronoamperometry. We propose that the mechanism for this improvement lies in the combination of several factors: i) a higher dispersion of platinum NPs, ii) an enhanced capacity of the Pt NPs to oxidize CO and iii) the continuous preconcentration of the reactant (HCOOH) within the zeolite microporosity occurring in solution. Finally, the preconcentration of other small organic molecules in hybrid catalyst should be also possible. This will be mainly controlled by the micropore size of zeolites and the molecular diameter of the reactant, as well as its affinity for the solvent.

5. Acknowledgements

This work was supported by French state funds managed by the ANR within the ‘‘Investissements d’Avenir’’ program (reference ANR-11-IDEX-0004-02) and more specifically within the frame-work of the Cluster of Excellence MATISSE.

Graphical Abstract

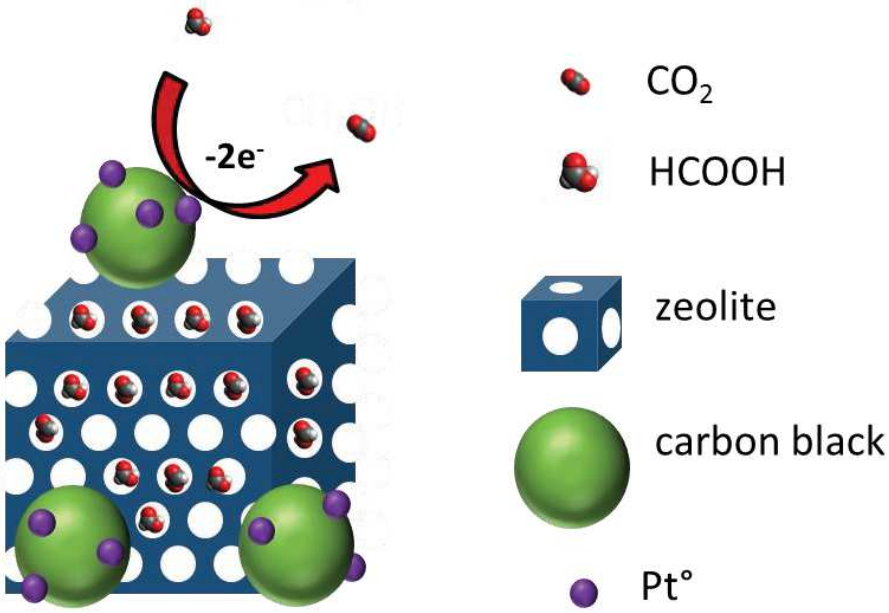

Figure captions

Fig. 1. SEM micrographs of size selected zeolite particles collected after centrifugation at 1500 rpm: (a) ZSM-5-NH_4^+, (b) ZSM-5-H^+) and as received carbon Vulcan XC-72R nanoparticles (c).

Fig. 2. X-Ray diffractograms of zeolites ZSM-5-H^+ and ZSM-5-NH_4^+ before and after prolonged aging by immersion in 0.5 M H_2SO_4 solution for 24h.

Fig. 3. TEM images of two different electrocatalytic inks containing Pt NPs (7 wt.%) + carbon Vulcan XC-72R + Nafion solution + two types of zeolites (18.5 wt.%). (a) ZSM-5-H^+ and (b) ZSM-5-NH_4^+. TEM images were taken after preparation and sonication of the ink for 15 min.

Fig. 4. Cyclic voltammetries in argon saturated 0.1 M HCOOH and 0.5 M H_2SO_4 solution (coloured curves) and in argon saturated 0.5 M H_2SO_4 solution (black curves) using different electrocatalytic inks: (a) 9 wt.% Pt/C (blue plot), (b) 7 wt.% Pt/18.5 wt.% ZSM-5-NH_4^+/C (red plot) and (c) 7 wt.% Pt/18.5 wt.% ZSM-5-H^+/C (green plot). Solid line represents the forward scan, whereas the backward scan is denoted by dashed lines. Scan rate 50 mV s^{-1}. Current density is calculated from the ECSA of Pt NPs present in the different electrocatalytic inks.

Fig. 5. Cyclic voltammetries in argon saturated 0.1 M HCOOH and 0.5 M H_2SO_4 solution using different electrocatalytic inks: 7 wt.% Pt/10 wt.% ZSM-5-NH_4^+/C (blue plot), 7 wt.% Pt/18.5 wt.% ZSM-5-NH_4^+/C (red plot) and 7 wt.% Pt/25 wt.% ZSM-5-NH_4^+/C (green plot). Scan rate 50 mV s^{-1}. Current density is calculated from the ECSA of Pt NPs present in the different electrocatalytic inks.

Fig. 6. Chronoamperometries in argon saturated 0.1 M HCOOH and 0.5 M H_2SO_4 solution of 9 wt.% Pt/C (blue plot), 7 wt.% Pt/18.5 wt.% ZSM-5-NH_4^+/C (red plot) and 7 wt.% Pt/18.5 wt.% ZSM-5-H^+/C (green plot). Applied potentials: (A) 0.54 V and (B) 0.74 V vs RHE.

Fig. 1

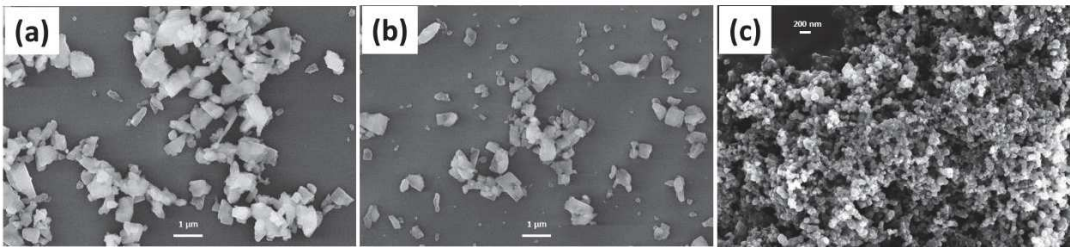

Fig. 2

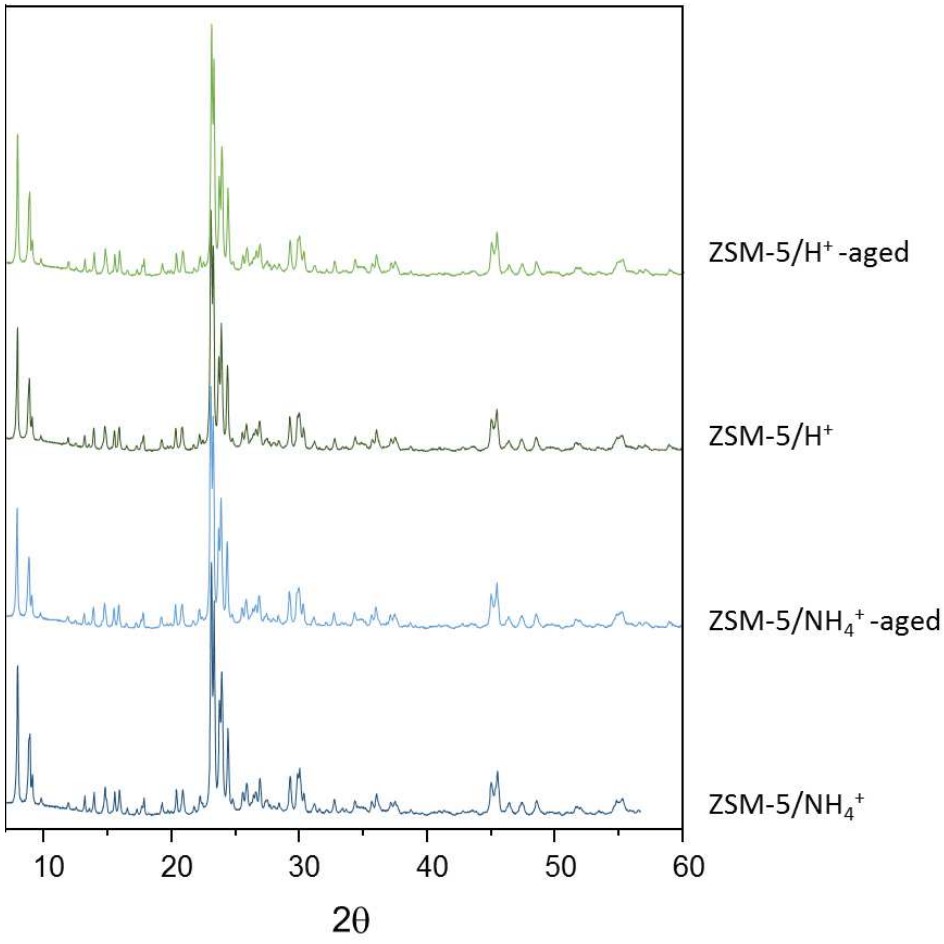

Fig. 3

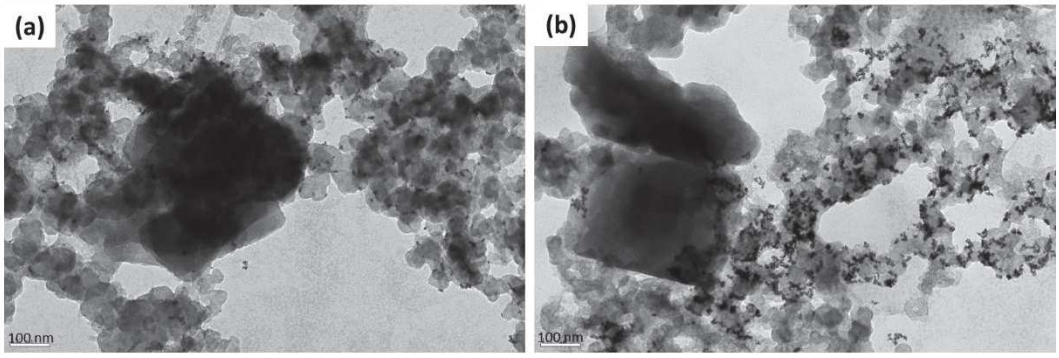

Fig. 4

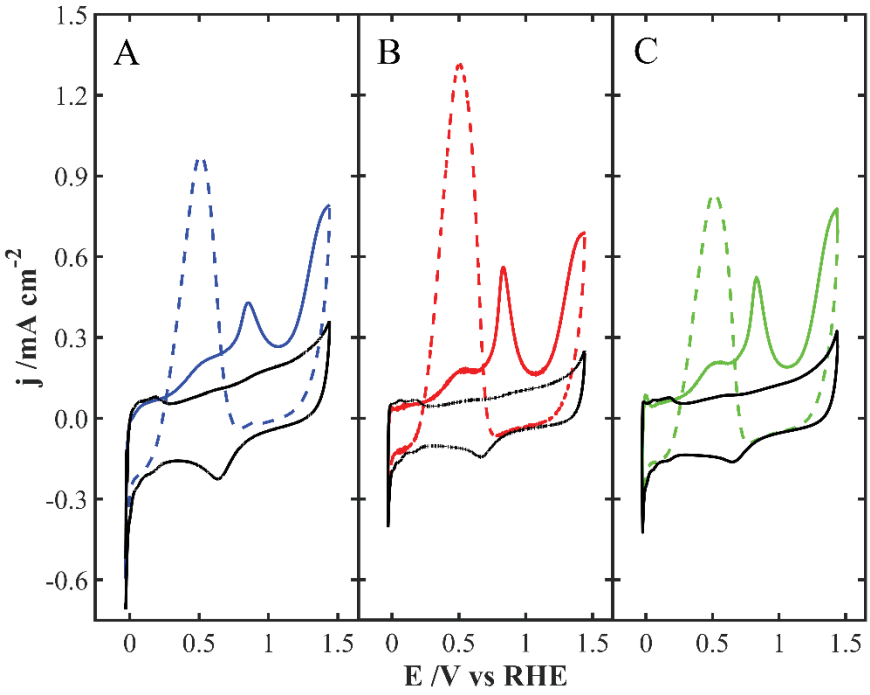

Fig. 5

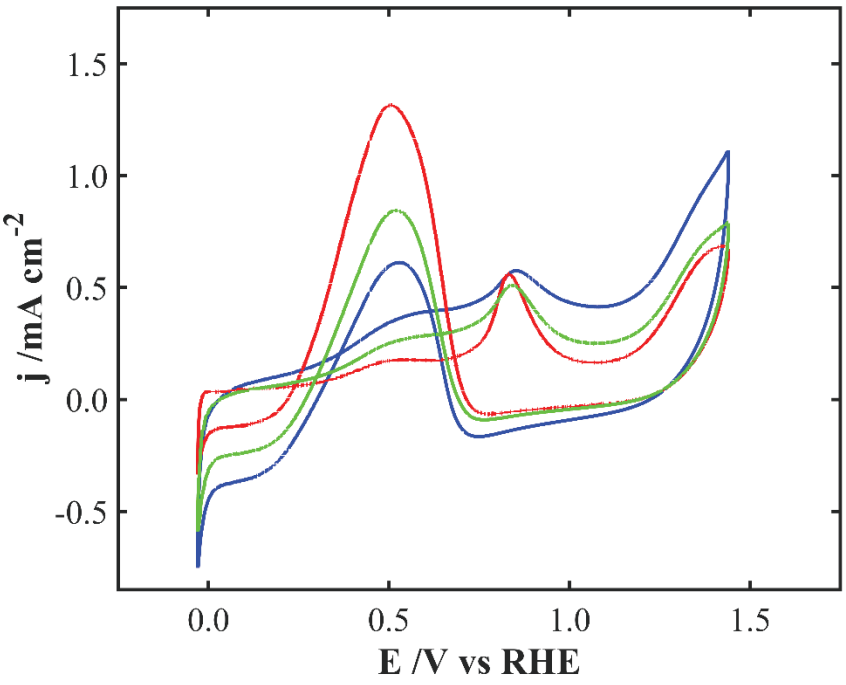

Fig. 6

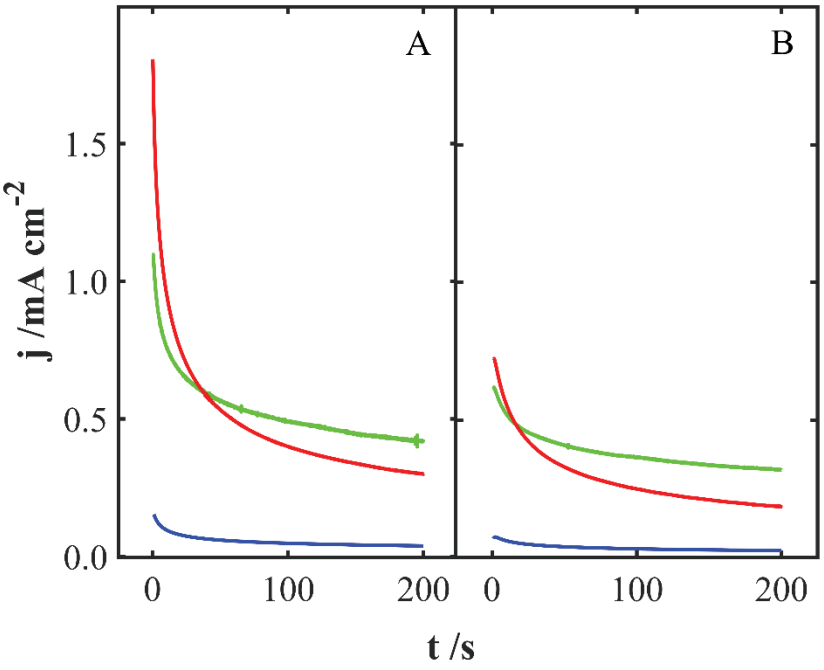

References

[1] J. Qiao, Y. Liu, F. Hong, J. Zhang, Chem. Soc. Rev. 43 (2014) 631–675.

[2] U.O. Nwabara, E.R. Cofell, S. Verma, E. Negro, P.J.A. Kenis, ChemSusChem. 13 (2020) 855–875.

[3] G. Díaz-Sainz, M. Alvarez-Guerra, J. Solla-Gullón, L. García-Cruz, V. Montiel, A. Irabien, J. CO2 Util. 34 (2019) 12–19.

[4] C. Rice, R.I. Ha, R.I. Masel, P. Waszczuk, A. Wieckowski, T. Barnard, J. Power Sources 111 (2002) 83.

[5] C. Rice, S. Ha, R.I. Masel, A. Wieckowski, J. Power Sources 115 (2003) 229.

[6] J.M. Feliu, E. Herrero, in: W. Vielstich, H. Gasteiger, A. Lamm (Eds.) Handbook of Fuel Cells - Fundamentals, Technology and Applications, vol. 2, John Wiley & Sons, Ltd., Chichester, 2003, pp. 625.

[7] P. Strasser, H. Ogasawara, Chemical Bonding at Surfaces and Interfaces. Chapter 6, Surface Electrochemistry, Elsevier, Amsterdam, The Netherlands 2008.

[8] M.T.M. Koper, Fuel Cell Catalysis: A Surface Science Approach, John Wiley & Sons, Hoboken, New Jersey, 2009.

[9] A. Capon, R. Parsons, J. Electroanal. Chem. & Interf. Electrochem. 44 (1973) 1.

[10] A. Capon, R. Parsons, J. Electroanal. Chem. & Interf. Electrochem. 44 (1973) 239.

[11] A. Capon, R. Parsons, J. Electroanal. Chem. & Interf. Electrochem. 45 (1973) 205.

[12] J. Solla-Gullón, V. Montiel, A. Aldaz, J. Clavilier, J. Electroanal. Chem. 491 (2000) 69.

[13] J. Solla-Gullón, F.J. Vidal-Iglesias, A. López-Cudero, E. Garnier, J.M. Feliu, A. Aldaz, Phys. Chem. Chem. Phys. 10 (2008) 3689.

[14] J.V. Perales-Rondón, E. Herrero, J. Solla-Gullón, C.M. Sánchez-Sánchez, J. Electroanal Chem. 793 (2017) 218.

[15] S. Zhang, Y. Shao, H.-G. Liao, J. Liu, I.A. Aksay, G. Yin, Y. Lin, Chem. Mater. 23 (2011) 1079.

[16] S.P.E. Smith, K.F. Ben-Dor, H.D. Abruna, Langmuir 15 (1999) 7325.

[17] A. Boronat-Gonzalez, E. Herrero, J.M. Feliu, J. Solid State Electrochem. 18 (2014) 1181.

[18] J.V. Perales-Rondón, J. Solla-Gullón, E. Herrero, C.M. Sánchez-Sánchez, Appl. Catal., B 201 (2017) 48.

[19] V. Grozovski, V. Climent, E. Herrero, J.M. Feliu, ChemPhysChem 10 (2009) 1922.

[20] V. Grozovski, V. Climent, E. Herrero, J.M. Feliu, Phys. Chem. Chem. Phys. 12 (2010) 8822.

[21] S. Kornic, M. Baker, Chem. Commun. (2002) 1700.

[22] N. Vilà, E. André, R. Ciganda, J. Ruiz, D. Astruc, A. Walcarius, Chem. Mater. 28 (2016) 2511.

[23] F. Yan, M. Wang, Q. Jin, H. Zhou, L. Xie, H. Tang, J. Liu, J. Electroanal. Chem. 881 (2021) 114969.

[24] A. Walcarius, E. Sibbotier, M. Etienne, J. Ghanbaja, Nat. Mater. 6 (2007) 602.

[25] D.R. Rolison, C.A. Bessel, Accounts of Chemical Research 33 (2000) 737.

[26] A. M. Rocco, K. V. Melo, C. J. de A. Mota, M. V. David and I. N. de Souza, Ionics, 25 (2019) 253.

[27] A. Suleiman, C. L. Menéndez, R. Polanco, E. R. Fachini, Y. Hernández-Lebrón, M. J.-F. Guinel, R. Roque-Malherbe and C. R. Cabrera, *RSC Adv.*, 5 (2015) 7637.

[28] A. Medina Ramirez, B. Ruiz Camacho, M. Villicaña Aguilera, I. R. Galindo Esquivel and J. J. Ramírez-Minguela, Appl. Surf. Sci., 456 (2018) 204.

[29] A. Medina Ramírez, M. Villicaña Aguilera, C. M. López-Badillo and B. Ruiz-Camacho, Int. J. Hydrog. Energy, 42 (2017) 30291.

[30] B. M. Daas and S. Ghosh, Electroanalysis, 29 (2017) 2516.

[31] B. M. Daas and S. Ghosh, J. Electroanal. Chem., 783 (2016) 308.

[32] S. Kavian, S. N. Azizi and S. Ghasemi, Int. J. Hydrog. Energy, 41 (2016) 14026.

[33] F. Alidusty, A. Nezamzadeh-Ejhieh, Int. J. Hydrog. Energy, 41 (2016) 6288.

[34] J. Yao and Y. Yao, Int. J. Hydrog. Energy, 41 (2016) 14747.

[35] C. G. Pope, J. Chem. Soc. Faraday Trans., 89 (1993) 1139.

[36] C. G. Pope, J. Chem. Soc. Faraday Trans., 92 (1996) 3647.

[37] T. C. Bowen, L. M. Vane, Langmuir 22 (2006) 3721

[38] H. Zhang, Y. Wang, P. Bai, X. Guo, X. Ni, J. Chem. Eng. Data 61 (2016) 213.

[39] E.E. Mallon, I.J. Babineau, J.I. Kranz, Y. Guefrachi, J.I. Siepmann, A. Bhan, M. Tsapatsis, J. Phys. Chem. B 115 (2011) 11431.

[40] M. León,T.D. Swift, V. Nikolakis, D.G. Vlachos, Langmuir 29 (2013) 6597.

[41] S. Bouden, A. Chaussé, S. Dorbes, O. El Tall, N. Bellakhal, M. Dachraoui, C. Vautrin-Ul, Talanta 106 (2013) 414.

[42] T. Nasir, N.A. Vodolazkaya, G. Herzog, A. Walcarius, Electroanalysis 31 (2019) 202.

[43] S.A. Rezvani, A. Soleymanpour, J. Chromat. A 1436 (2016) 34.

[44] M. Hernandez-Valez, R. Roque-Malherbe, J. Mater. Science Lett. 14 (1995) 1112.

[45] M. Vasić, M. Čebela, I. Pašti, L. Amaral, R. Hercigonja, D. M. F. Santos and B. Šljukić, Electrochim. Acta, 259 (2018) 882.

[46] S. Trasatti, O.A. Petrii, Pure Appl. Chem. 63 (1991) 711.

[47] R. Woods, Chemisorption at electrodes, in: A.J. Bard (Ed.), Electroanalytical Chemistry, 9, Marcel Dekker, New York, 1976.

[48] D. Y. Chung, K.-J. Lee and Y.-E. Sung, J. Phys. Chem. C, 120 (2016) 9028.

[49] F.A. Hanc-Scherer, C.M. Sanchez-Sanchez, P. Ilea, E. Herrero, ACS Catal. 3 (2013) 2935.

[50] J.V. Perales-Rondón, S. Brimaud, J. Solla-Gullón, E. Herrero, R. Jürgen Behm, J.M. Feliu, Electrochim. Acta 180 (2015) 479.

[51] J.V. Perales-Rondon, E. Herrero, J.M. Feliu, Electrochim. Acta 140 (2014) 511.

Author contributions

Juliette Blanchard, Carlos M. Sanchez-Sanchez: Methodology, Resources, Validation, Supervision; **Carlos M. Sanchez-Sanchez:** Conceptualization; **Juliette Blanchard, Juan V. Perales-Rondón, Carlos M. Sanchez-Sanchez:** Formal analysis; **Juliette Blanchard, Carlos M. Sanchez-Sanchez:** Funding acquisition; **Lu Zhang, Angélica Thomère:** Investigation, Roles/Writing - original draft; **Carlos M. Sanchez-Sanchez:** Project administration; **Juliette Blanchard, Juan V. Perales-Rondón, Carlos M. Sanchez-Sanchez:** Visualization; **Juliette Blanchard, Juan V. Perales-Rondón, Carlos M. Sanchez-Sanchez:** Writing - review & editing. All authors have read and approved the final version of the manuscript.

Declaration of interests

☒ The authors declare that they have no known competing financial interests or personal relationships that could have appeared to influence the work reported in this paper.

☐The authors declare the following financial interests/personal relationships which may be considered as potential competing interests:

Platinum-zeolite hybrid catalyst for the electrooxidation of formic acid

Lu Zhang[a,b], *Juan V. Perales-Rondón*[a,c], *Angélica Thomère*[a,b], *Juliette Blanchard*[b], *Carlos M. Sánchez-Sánchez**[,a],

[a]*Sorbonne Université, CNRS, Laboratoire Interfaces et Systèmes Electrochimiques, 4 place Jussieu, F-75005 Paris, France*

[b]*Sorbonne Université, CNRS, Laboratoire de Réactivité de Surface, LRS UMR 7197, F-75005, Paris, France.*

[c]*Instituto Universitario de Electroquímica, Universidad de Alicante, Ap. 99, 03080, Alicante, Spain*

Abstract

Formic acid oxidation reaction (FAOR) was studied using different platinum-zeolites hybrid catalysts. The catalysts were prepared by addition of two different forms of the ZSM-5 zeolite (ZSM-5-H^+ and ZSM-5-NH_4^+) to an ink containing Vulcan carbon support and Pt nanoparticles (NPs). TEM images demonstrate a proper mixture of the components in the ink and a good dispersion of the Pt NPs mainly over the carbon. Both zeolites (ZSM-5-NH_4^+ and ZSM-5-H^+) are stable under electrochemical conditions for FAOR, but ZSM-5-NH_4^+ undergoes fast conversion into ZSM-5-H^+ due to the exchange between the compensator cation in the zeolite and protons in solution.

A significant enhancement on the catalytic activity was found for both zeolite hybrid catalysts, being the ink containing ZSM-5-H^+ the more stable over time. In particular, 7

and 10 times larger current densities than on 9 wt.% Pt/C were achieved by the (7 wt.% Pt/18.5 wt.% ZSM-5-NH_4^+/C) and the (7 wt.% Pt/18.5 wt.% ZSM-5-H^+/C) catalysts in chronoamperometry, respectively. The results demonstrated the beneficial and synergetic effect of the addition of zeolites in order to improve the catalytic activity of Pt NPs. The addition of zeolite ZSM-5 within the electrocatalyst did not provoke any relevant modification in the type of features displayed in cyclic voltammetry, but provoked a significant enhancement of the peak current density associated with the CO stripping. We propose that the mechanism for this improvement lies in a more efficient distribution of Pt nanoparticles on the catalytic ink thanks to the presence of zeolites and the preconcentration of the reactant (HCOOH) within the zeolite microporosity occurring in solution. Moreover, local pH modifications associated with the NH_4^+/H^+ exchange could have some impact on the kinetics of the FAOR by the *direct via*.

Keywords

Hybrid catalyst; zeolites; preconcentration; Formic acid oxidation; Pt nanoparticles.

1. Introduction

Nowadays a lot of effort is concentrated on developing large scale electrochemical systems for formic acid (HCOOH) production as an efficient and feasible method to recycle CO_2 from the atmosphere [1-3]. In the same context, electrooxidation of formic acid represents a relevant reaction to recover the electrical energy stocked in that molecule and direct formic acid fuel cells (DFAFCs) have been proposed to be used as small power suppliers in electronic devices [4-6]. As a fuel, formic acid presents fast oxidation kinetics, less fuel crossover through the ion exchange membrane compared with other fuels such as methanol, and is also easy to handle and manipulate once produced. Additionally,

formic acid oxidation reaction (FAOR) is one of the most studied reactions in electrocatalysis, since it can be used as a model in fundamental studies of reaction mechanism for small organic molecules (SOM) [7]. More specifically, formic acid oxidation on platinum electrodes has been widely studied over the last two decades [8], because of the high activity of this metal for the oxidation of organic molecules. Furthermore, the comprehension of the reaction mechanism on this metal can be extrapolated to other important metallic catalysts.

It is well known in the literature that formic acid oxidation on platinum electrodes presents two different reaction pathways [9-11]. The first one is the so-called *indirect via*, which involves the initial formation of adsorbed CO that acts as a poison intermediate followed by its subsequent oxidation to CO_2 at higher overpotential values. The second pathway is known as the *direct via*, and implies the formation of an active intermediate, which is immediately oxidized into CO_2 at lower overpotential values.

Different methods have been used to improve the performance of Pt catalysts to FAOR. One of them is based on increasing the amount of highly active specific crystallographic sites on the electrode surface by controlling size and/or shape of nanoparticles (NPs) [12,13]. Another method to enhance Pt specific activity is to modify the chemical composition of the Pt catalyst by either forming an alloy with other d-band metals such as Pd, Au or Ru [14,15] or adding a foreign adatom such as Bi, Sb or Pb [16-18], which might be adsorbed and deposited as a sub-monolayer. In both cases, a relevant effect on the FAOR mechanism is produced by strongly supressing the CO formation and/or promoting the FAOR by the direct via [19,20].

Zeolites are very useful materials in heterogeneous catalysis, but have been mainly used at the solid/gas interface. Zeolites are microporous crystalline aluminosilicates

(SiO_2/Al_2O_3) that provides a high surface area and molecular-sized cavities (cavities with sizes in the range 0.3-1.2 nm). The zeolite pore dimension allows physical exclusion or inclusion of specific molecules or ions. In fact, size exclusion plays a major role in adsorption of molecules within the microporosity of zeolites. A few examples have been already reported in the literature taking advantage of this physical exclusion property in electrocatalysis. For instance, different thin films of Na zeolite A (4 Å pore size) and K zeolite A (3 Å pore size) have been synthesized on conducting SnO_2 electrodes for behaving as a nanoporous filter in an electrochemical environment [21]. The Na zeolite A film let pass specific molecules such as molecular oxygen (3.145 Å molecular dimeter) to the electrode surface and simultaneously reject larger diameter interference species by size exclusion. Nevertheless, the diffusion coefficient of oxygen gets reduced by two orders of magnitude within the zeolite pores, which reduces the limiting current for oxygen reduction reaction that can be achieved. A similar approach has been also explored on mesoporous (2-3 nm in diameter) silica films grown on electrodes [22-24]. In addition to the sub-nanometer filters application, zeolites modified with redox-active guests [25] and zeolite particles mixed together with the catalyst for the electrochemical oxidation of small organic molecules [26-34] have also exhibited interesting results in different electrochemical systems. Different types of zeolites have been used as support for metallic nanoparticles in widely studied electrocatalytic reactions such as methanol [26-28] and formaldehyde oxidation reactions [32]. In most cases, zeolites have a positive impact on the electrochemical activity (by decreasing the onset potential and increasing the oxidation current) [28]. Several possible causes have been already proposed in the literature for explaining this activity enhancement: a lower ohmic drop (thanks to the hydrophilic nature of zeolites), a higher tolerance of Pt NPs to CO (because of a modification of the electronic density of Pt NPs by the zeolite), a higher dispersion of

platinum, an enhanced capability of the Pt NPs to oxidize CO (thanks to the oxygen-rich environment of zeolites) [28, 32]. Nevertheless, the electroactive species preconcentration within the zeolite microporosity was never proposed before, although the adsorption of small organic molecules, such as alcohols and carboxylic acids, from diluted aqueous solutions within the porosity of zeolites (including zeolite Socony Mobil-5 (ZSM-5)) is well established [35-40]. Moreover, several authors has proposed zeolite adsorption as an efficient separation method for recovering those organic molecules from aqueous effluents [38].

A conventional approach to improve the sensitivity in electroanalysis of trace metals is the analyte preconcentration [41]. Preconcentration electroanalysis of paraquat, a pesticide, by electrostatic binding to mesoporous silica has been previously reported [42] and zeolites have been already used for ex-situ preconcentration by solid phase extraction [43], but never for in-situ preconcentration, which is the main goal of the present work.

Exploring the adsorption in zeolites at the solid-liquid interface requires to take into consideration the hydrophilicity/hydrophobicity of zeolites, which is governed by the Si/Al ratio. For electrochemical applications in aqueous solutions, only zeolites such as faujasite, ZSM-5 and beta, with moderately high Si/Al ratio (hydrophilic zeolites, Si/Al<40), can be envisaged, because strongly hydrophobic zeolites present almost zero water adsorption capacity making them poorly efficient in electrochemical conditions. In these hydrophilic zeolites, solute and solvent molecules may compete for the adsorption sites within the micropores, as has been already demonstrated for ethanol and acetic acid aqueous solutions adsorbed on ZSM-5 [37]. However, the adsorption within the zeolite is not only controlled by the molecule size, but also by the affinity of the solute for the solvent vs. the zeolite cavities. Experimental isotherms can be fitted using different adsorption models depending on the type of organic molecule in solution [39]. In

particular, high silica zeolites such as ZSM-5 have been shown to be effective for the adsorption of formic and/or acetic acids [35, 37-38, 40]. Adsorption isotherms for formic acid aqueous solutions have been already reported in the beta zeolite (SiO_2/Al_2O_3 = 18) and co-adsorption of formic acid and water following the isotherm type Freundlich has been established [40].

Despite the fact that zeolites are insulator materials, hydrated zeolites present an inter- and intra-crystallite cationic conduction, because they behave as an electrolyte, thanks to the water adsorbed in their cavities [25, 44]. Additionally, the presence of metallic nanoparticles in their pores can also increase their conductivity by several orders of magnitude [45]. With this picture in mind, the objective of the present work is to show the potential of local preconcentration of electroactive species (formic acid, molecular diameter 3.81 Å) within the electrode interface using zeolite ZSM-5 (channel diameter 5-6 Å) as one of the components within the catalytic ink forming the (Pt/ZSM-5/Carbon) hybrid catalyst for FAOR in acidic media and to establish the feasibility of using such materials for conferring higher catalytic activity and stability to real DFAFCs.

2. Material and methods

2.1.Preparation of the electrocatalytic ink

Commercial colloidal Pt spherical nanoparticles (0.05 mg Pt/mL) with average size of 4 nm were supplied by Metrohm-DropSens. Commercial zeolite ZSM-5-NH_4^+ (specific surface = 425 $m^2 \cdot g^{-1}$, particle size distribution < 4.2 μm), (SiO_2:Al_2O_3 = 28:1) was supplied by Alfa-Aesar. Zeolite ZSM-5-H^+ was obtained after calcination of ZSM-5-NH_4^+ in a muffle furnace for 5h at 500ºC in air (SiO_2:Al_2O_3 = 28:1). A size selection on zeolite particles was operated in order to obtain suspensions of zeolite particles with a

reasonable stability over time (stability of ca. 1h) and to ensure a good contact between the components of the hybrid electrode. This size selection was achieved by selectively removing larger particles (size >1 μm) from an isopropanol/zeolite suspension using centrifugation at 1500 rpm. SEM micrographs of size-selected ZSM-5-NH_4^+ and ZSM-5-H^+ are shown in Figure 1. Commercially available carbon Vulcan XC-72R, a conductive carbon black from Cabot Co. with an average particle size of 50 nm (see Figure 1), was used as carbon support. Nafion solution 5% w/w in a mixture of lower aliphatic alcohols and water was employed as ionic conductor.

The colloidal suspension of platinum NPs, carbon and ethanol were mixed together and sonicated for 90 min. The isopropanol suspension containing the zeolite ZSM-5 particles was pretreated with ultrasound for 10 minutes and then added to the previous suspension. The resulting suspension was treated with ultrasound for half an hour before addition of diluted Nafion solution (1:9 v/v in ethanol). The final suspension (electrocatalytic ink) was treated with ultrasound for another 15 minutes before dropping 4 μL on a glassy carbon disc electrode (diameter = 3 mm) used as current collector and dried for 30 min. Several ink compositions were evaluated herein: (9 wt.% Pt/C), (7 wt.% Pt/10 wt.% ZSM-5-NH_4^+/C), (7 wt.% Pt/18.5 wt.% ZSM-5-NH_4^+/C), (7 wt.% Pt/25 wt.% ZSM-5-NH_4^+/C) and (7 wt.% Pt/18.5 wt.% ZSM-5-H^+/C).

2.2.Zeolites stability tests in acid solution

In order to investigate the chemical and structural stability of the zeolite ZSM-5 immersed in acid aqueous solution under electrocatalytic conditions, 1g of zeolite (either ZSM-5-NH_4^+ or ZSM-5-H^+) was suspended in a 0.5 M H_2SO_4 solution and the suspension was stirred during 24h. The solid phase was recovered by centrifugation, washed 3 times

with distilled water and dried in the oven at 50°C during 1 night before evaluating the effect of that treatment on the zeolite crystallinity and amount of acid catalytic sites.

2.3.Physicochemical characterization

Crystallinity of zeolites was investigated using X-ray diffraction (XRD) with a Bruker D8 ADVANCE diffractometer (Cu Kα radiation) over a 2θ range from 5° to 80° with a step size of 0.02° and a counting time of 0.5 s per step. Chemical composition of zeolites (ratio SiO_2/Al_2O_3) was determined using X-ray fluorescence (XRF) analysis; experiments were conducted under He flow with an energy dispersive spectrometer (XEPOS with Turboquant powder software) equipped with a 50-Watt end-window X-ray tube. In addition to this, the extent of NH_4^+/H^+ exchange between the compensator cation in the zeolite ZSM-5-NH_4^+ and the protons in solution was estimated based on thermodesorption experiments followed by mass spectrometer. About 0.3 g of zeolite ZSM-5-NH_4^+ were heated under He flow (25 ml min^{-1}) from RT to 700°C. NH_3-desorption was monitored by following m/z=15 -corresponding to NH- and the amount of desorb NH_3 was estimated by integrating the desorption peak and using a calibration curve performed by injecting NH_3 pulses of known volume.

The morphology and size of the zeolites and carbon Vulcan XC-72R were characterized using scanning electron microscopy (SEM) (Zeiss, Supra 55 microscope). Moreover, transmission electron microscopy (TEM) measurements were performed to estimate both particle size and distribution of all 3 components present in the electrocatalytic ink. Experiments were performed using a JEOL 2010 microscope operating at 200 kV with a LaB_6 filament and equipped with an Orius CCD camera (Gatan).

2.4.Electrochemical characterization

Cyclic voltammetry (CV) and chronoamperometry (CA) were performed using a conventional electrochemical glass cell of 3 electrodes at room temperature and a potentiostat (either CHI 760E or CHI 920D). The working electrode was prepared by drop casting 4 µL of each electrocatalytic ink on a 3 mm diameter glassy carbon disc electrode. A platinum wire (d = 0.5 mm) was used as a counter electrode, and Hg/Hg_2SO_4 within a Luggin capillary was employed as a reference electrode. All potentials used in this work were converted to *RHE* ($E_{Hg/Hg2SO4}$ = +0.64 V vs RHE).

CVs for evaluating the electrochemical surface area (ECSA) of Pt in the different electrocatalytic inks were carried out in a 0.5 M H_2SO_4 (Sigma-Aldrich TraceSELECT 95%) solution deaerated with Ar (N60, Air Liquide). The ECSA value was determined by quantifying the charge involved in the voltammetric peaks corresponding to the hydrogen desorption within the hydrogen underpotential deposition region (between 0.05 and 0.35 V/RHE) after subtraction of the double layer contribution [46]. 210 µC cm^{-2} was adopted as the calibration charge density for desorption of a complete monolayer of H atoms on polyoriented Pt electrodes [47]. CVs and CAs for studying the electrocatalytic activity for FAOR were carried out in deaerated 0.1 M HCOOH (Merck KGaG 98 %) and 0.5 M H_2SO_4 solution. An electrochemical pre-treatment for removing the CO_{ads} accumulated at the electrode surface from previous FAOR experiments was performed before starting each CA. This consists in holding the electrode potential at 0.95 V vs RHE for 5 s.

3. Results and discussion

ZSM-5 zeolite immersed in solution under electrochemical conditions for performing FAOR may undergo numerous modifications. Indeed, the acid pH solution used for the reaction may provoke several effects: (i) zeolite may not be fully stable in these conditions and an amorphous phase could be developed; (ii) extraction of framework aluminum could occur, leading to a decrease in the number of acid sites; (iii) for the ammonium form of the zeolite, NH_4^+ cations may be ion exchanged by the protons in solution. In order to investigate all these potential modifications, zeolite samples have been aged under electrochemical conditions and characterized in terms of stability /amorphisation (XRD), extraction of aluminum atoms (XRF) and NH_4^+ content (thermal desorption of NH_3).

The X-ray diffractograms of the fresh and aged ZSM-5 zeolites are shown in Figure 2. All four diffractograms are identical and no amorphous phase is detected. This indicates that neither the calcination step (used to convert ZSM-5-NH_4^+ into ZSM-5-H^+) nor the aging in acidic solution (24 h immersion in 0.5 M H_2SO_4 solution) induces a detectable amorphisation of the zeolite. X-ray fluorescence analysis proves that the two fresh zeolites have the same chemical composition (SiO_2:Al_2O_3 = 28:1) and the composition of the two zeolites are only very marginally modified after a prolonged aging in acidic solution (SiO_2:Al_2O_3 = 30:1), indicating that a very small fraction of Al atoms are extracted from the zeolite framework. Moreover, for the ZSM-5-NH_4^+ case, the aged zeolite was further compared to the starting zeolite in order to evaluate the extent of H^+/NH_4^+ exchange produced in acidic solution. NH_4^+ titration by thermodesorption indicates that about 84% of NH_4^+ are ion-exchanged by protons after immersion in acidic solution for 2h. Thus, both zeolites (ZSM-5-NH_4^+ and ZSM-5-H^+) are stable under

electrochemical conditions for FAOR, but ZSM-5-NH_4^+ undergoes fast conversion into ZSM-5-H^+ due to the exchange between the compensator cation in the zeolite and protons in solution.

The addition of ZSM-5 zeolites could provide a synergetic effect in the catalytic activity of conventional Pt/C catalysts for FAOR. With the aim of demonstrating such a statement, a systematic study of FAOR activity of different Pt electrocatalytic inks was performed. Figure 3 shows the TEM micrographs of two different hybrid catalytic inks studied in this work, prepared adding Pt NPs, carbon support (Vulcan XC-72R) and either ZSM-5-H^+ (Figure 3a) or ZSM-5-NH_4^+ (Figure 3b) zeolites. On both images, one clearly observes that Pt NPs are supported on the carbon particles. This was expected considering that the size of the Pt NPs (4 nm) does not allow them to enter the zeolite micropores (5 Å). One can also observe that carbon particles are well interconnected with the zeolites. Moreover, TEM images show a good dispersion of the Pt NPs on the carbon support. This structure ensures an ideal access of both reactant and electrolyte to the Pt electrocatalyst.

Figure 4a shows the conventional cyclic voltammetry for FAOR on Pt NPs supported on carbon (blue plot) compared with the blank in the absence of HCOOH in solution (black plot). This type of voltammogram has been extensively described in the literature [[48]], since Pt exhibits common electrochemical features oxidizing different small organic molecules [[49]]. The main features within the positive-going sweep (blue solid line in Figure 4a) correspond to the so-called *indirect via*, which involves the formation of adsorbed CO from HCOOH dehydration that poisons the metallic sites. The onset of the oxidation peak centred at 0.85 V vs RHE corresponds to the start of the stripping of CO_{ads} by OH_{ads}, which becomes the rate determining step of the FAOR. Higher potential values than the CO stripping peak provoke the increased coverage of Pt surface by adsorbed OH and subsequent Pt surface oxidation. In contrast, the main feature

on the negative-going sweep (blue dashed line in Figure 4a) corresponds to a high activity oxidation peak centred at 0.5 V vs RHE, which can be assigned to the FAOR by the *direct via*, coupled to the reduction of the Pt oxide (peak centred at 0.65 V vs RHE and shown in the black plot in Figure 4a) previously formed during the positive-going sweep.

The addition of zeolite ZSM-5 within the electrocatalyst allows a higher dispersion of Pt NPs, which is demonstrated by comparing ECSA values calculated from the cyclic voltammograms in the absence of HCOOH in solution (black plots in Figure 4). ECSA values for Pt-zeolite hybrid catalysts are 3 times larger than for Pt/C. However, this difference is already taken into account when comparing the FAOR activity displayed by those catalysts in Figure 4, since specific current density is reported. Figures 4b and c display the cyclic voltammetry for FAOR corresponding to two different Pt-zeolites hybrid catalysts. The addition of ZSM-5 does not provoke any relevant modification in the type of features displayed by the CV, but provokes a significant enhancement of the peak current density associated with the CO stripping at 0.85 V (figures 4b and c) in comparison with the one displayed by Pt/C (figure 4a). Moreover, in the ZSM-5-NH_4^+ case, a significant enhancement of FAOR by the *direct via* is also observed on the negative-going sweep (figure 4b). This behaviour can be explained by the exchange between the compensator cation in the zeolite ZSM-5-NH_4^+ and protons in solution, which does not happen when ZSM-5-H^+ participates in the hybrid electrocatalyst. As has been stated in the literature, FAOR is highly dependent on solution pH [50-51]. Hence, local pH modifications due to the NH_4^+/H^+ exchange could have some impact on the kinetics of the FAOR by the *direct via*.

The oxidation current density enhancement associated with the CO stripping at 0.85 V displayed by the Pt-zeolites hybrid catalysts, which cannot be associated with a change in the reaction mechanism, is compatible with a higher local concentration of HCOOH

within the diffusion layer of the electrode due to the release of HCOOH previously preconcentrated within the microporosity of ZSM-5. This preconcentration step most likely happens within the time gap devoted to deoxygenation of the solution by argon bubbling before starting the electrochemical measurements on the electrocatalyst, but continues meanwhile the electrode is immersed in solution, since zeolite particles are continuously exposed to 0.1 M HCOOH in solution. Moreover, several previous works have demonstrated that Pt catalysts supported on zeolite present a major tolerance to the CO formation on the catalyst surface, due to the intrinsic capability of zeolites to facilitate CO reaction with OH groups [25, 30-31].

The percentage of zeolite in the electrodes characterized by cyclic voltammetry on Figure 4b and c was 18.5 wt.%. This zeolite loading was selected after testing different catalysts prepared with different amounts of zeolite. Figure 5 shows the overlay of cyclic voltammograms for FAOR of 3 different hybrid catalysts containing 10, 18.5 and 25 wt. % of ZSM-5-NH_4^+ in their composition. Figure 5 shows that 18.5 wt. % of zeolite corresponds to an optimum loading in terms of HCOOH oxidation current density by the direct via and at the CO stripping peak at ca. 0.85 V. The decrease in current observed at higher percentage of zeolites (25 wt. %) can be assigned to an increase in the ohmic drop within the hybrid catalyst due to the insulator nature of zeolites. In contrast, the decrease in current observed at low zeolite loading (10 wt. %) indicates that the zeolite content is too low to improve significantly the catalytic activity.

One way to evaluate the stability of an electrocatalyst is to perform chronoamperometries at specific potentials. Figure 6 shows the chronoamperometric curves at two different applied potentials (0.54 and 0.74 V vs RHE) for conventional Pt/C catalyst and the two Pt-zeolite hybrid catalysts (9 wt.% Pt/C, 7 wt.% Pt/18.5 wt.% ZSM-5-NH_4^+/C and 7 wt.% Pt/18.5 wt.% ZSM-5-H^+/C). As can be expected, for the three

samples, the current densities are larger at 0.54 V than at 0.74 V and undergo slow decrease over time following Cotrell equation, as expected for a macroelectrode. After 200 s a pseudo-steady state is reached for all samples. Moreover, the two Pt-zeolite hybrid catalysts produce a significantly higher current density than the Pt/C catalyst. In particular, 7 and 10 times larger current densities at pseudo steady-state are achieved by the 7 wt.% Pt/18.5 wt.% ZSM-5-NH_4^+/C and the 7 wt.% Pt/18.5 wt.% ZSM-5-H^+/C catalysts, respectively. When comparing the behaviour of the two Pt-zeolite hybrid catalysts, it is clear that, although ZSM-5-NH_4^+ (red plot in Figure 6) present higher initial current densities, the hybrid catalyst containing ZSM-5-H^+ (green plot in Figure 6) displays a more stable activity for FAOR, since the rate at which the current density decreases is slower than in the case of ZSM-5-NH_4^+. This fact is probably due to the local pH modification associated with the exchange between the compensator cation in the zeolite ZSM-5-NH_4^+ and protons in solution.

The results shown in Figures 4 and 6 evidence that the incorporation of ZSM-5 as a part of the electrocatalyst improves the catalytic activity of Pt NPs for FAOR when compared with a conventional Pt-NPs/C electrocatalyst. Enhancement of the catalytic activity for the oxidation of different small organic molecules on Pt NPs-based electrodes upon addition of zeolite has already been previously observed. However, in most of the previous studies, Pt NPs where located within the zeolite porosity. This is however not the case in the present study as the size of the preformed Pt NPs used for the preparation of the electrocatalyst (about 4 nm) does not allow them to enter the pores of ZSM-5 (ca 5 Å). This affirmation is confirmed by the TEM micrographs of the corresponding inks (Figure 3) that clearly establish that the Pt NPs are located on the carbon particles. Hence, some of the hypotheses initially listed regarding the promoting role of zeolite should be reconsidered. For example, one can exclude a modification of the electronic properties of

the Pt NPs by the presence of zeolite particles in the hybrid catalyst. However, a more efficient distribution of Pt NPs on the hybrid catalysts have been confirmed in this work. Thus, we propose an additional hypothesis based on the excellent adsorption properties of high silica zeolites for formic or acetic acids in aqueous solution, which are well documented in the literature [35, 37-38, 40]. In principle, either reactant (HCOOH) preconcentration or products (CO_2) adsorption within the microporosity of ZSM-5 can contribute to justify the significant current density enhancement observed in hybrid catalysts by cyclic voltammetry and chronoamperometry. In both cases, diffusion of species is necessary, either HCOOH diffusion from the zeolite microporosity to the solution in the vicinity of Pt NPs or CO_2 diffusion from the Pt surface towards the zeolite. Nevertheless, the concentration gradient established by the HCOOH consumption within the diffusion layer of the hybrid electrode drives HCOOH out of the zeolite, which is not the case for CO_2, since the concentration gradient drives CO_2 into the bulk solution. For this reason, we propose a continuous local preconcentration of HCOOH (molecular diameter 3.81 Å) within ZSM-5 (microporosity size 5-6 Å) as one of the dominant effects enhancing catalytic activity reported here for FAOR on hybrid Pt-zeolite catalysts.

4. Conclusions

We present here platinum-zeolites hybrid catalysts prepared using two different zeolites (ZSM-5-H^+ and ZSM-5-NH_4^+) and three different loading of ZSM-5 (10, 18.5 and 25 wt. %). The characterization of the hybrid catalysts showed a good homogeneity of the composites (good distribution of ZSM-5 and carbon Vulcan NPs), Pt NPs essentially located on the carbon support and a more efficient dispersion of the Pt NPs in comparison with Pt/C. The stability tests performed on the ZSM-5 particles immersed in solution under electrochemical conditions indicated a good stability of the zeolite particles

(absence of amorphisation and moderate extraction of framework aluminium atoms). This conclusion is supported by comparing XRD, XRF and NH_3 thermodesorption data performed on fresh and aged samples. The presence of zeolites improves not only the catalytic activity, but also the stability of both hybrid catalysts, being that containing ZSM-5-H^+ the more stable on time, as demonstrated by chronoamperometry. We propose that the mechanism for this improvement lies in the combination of several factors: i) a higher dispersion of platinum NPs, ii) an enhanced capacity of the Pt NPs to oxidize CO and iii) the continuous preconcentration of the reactant (HCOOH) within the zeolite microporosity occurring in solution. Finally, the preconcentration of other small organic molecules in hybrid catalyst should be also possible. This will be mainly controlled by the micropore size of zeolites and the molecular diameter of the reactant, as well as its affinity for the solvent.

5. Acknowledgements

This work was supported by French state funds managed by the ANR within the ‘‘Investissements d’Avenir’’ program (reference ANR-11-IDEX-0004-02) and more specifically within the frame-work of the Cluster of Excellence MATISSE.

Graphical Abstract

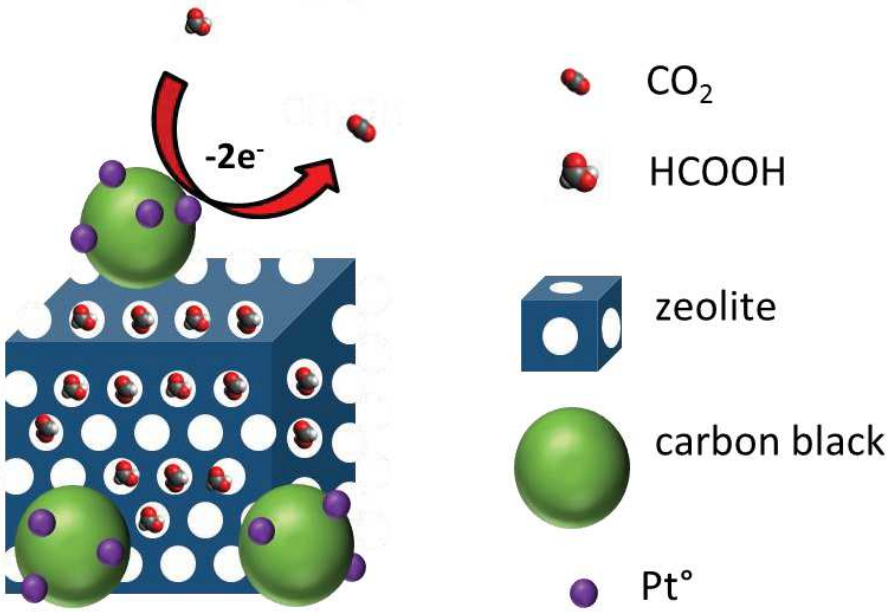

Figure captions

Fig. 1. SEM micrographs of size selected zeolite particles collected after centrifugation at 1500 rpm: (a) ZSM-5-NH_4^+, (b) ZSM-5-H^+) and as received carbon Vulcan XC-72R nanoparticles (c).

Fig. 2. X-Ray diffractograms of zeolites ZSM-5-H^+ and ZSM-5-NH_4^+ before and after prolonged aging by immersion in 0.5 M H_2SO_4 solution for 24h.

Fig. 3. TEM images of two different electrocatalytic inks containing Pt NPs (7 wt.%) + carbon Vulcan XC-72R + Nafion solution + two types of zeolites (18.5 wt.%). (a) ZSM-5-H^+ and (b) ZSM-5-NH_4^+. TEM images were taken after preparation and sonication of the ink for 15 min.

Fig. 4. Cyclic voltammetries in argon saturated 0.1 M HCOOH and 0.5 M H_2SO_4 solution (coloured curves) and in argon saturated 0.5 M H_2SO_4 solution (black curves) using different electrocatalytic inks: (a) 9 wt.% Pt/C (blue plot), (b) 7 wt.% Pt/18.5 wt.% ZSM-5-NH_4^+/C (red plot) and (c) 7 wt.% Pt/18.5 wt.% ZSM-5-H^+/C (green plot). Solid line represents the forward scan, whereas the backward scan is denoted by dashed lines. Scan rate 50 mV s^{-1}. Current density is calculated from the ECSA of Pt NPs present in the different electrocatalytic inks.

Fig. 5. Cyclic voltammetries in argon saturated 0.1 M HCOOH and 0.5 M H_2SO_4 solution using different electrocatalytic inks: 7 wt.% Pt/10 wt.% ZSM-5-NH_4^+/C (blue plot), 7 wt.% Pt/18.5 wt.% ZSM-5-NH_4^+/C (red plot) and 7 wt.% Pt/25 wt.% ZSM-5-NH_4^+/C (green plot). Scan rate 50 mV s^{-1}. Current density is calculated from the ECSA of Pt NPs present in the different electrocatalytic inks.

Fig. 6. Chronoamperometries in argon saturated 0.1 M HCOOH and 0.5 M H_2SO_4 solution of 9 wt.% Pt/C (blue plot), 7 wt.% Pt/18.5 wt.% ZSM-5-NH_4^+/C (red plot) and 7 wt.% Pt/18.5 wt.% ZSM-5-H^+/C (green plot). Applied potentials: (A) 0.54 V and (B) 0.74 V vs RHE.

Fig. 1

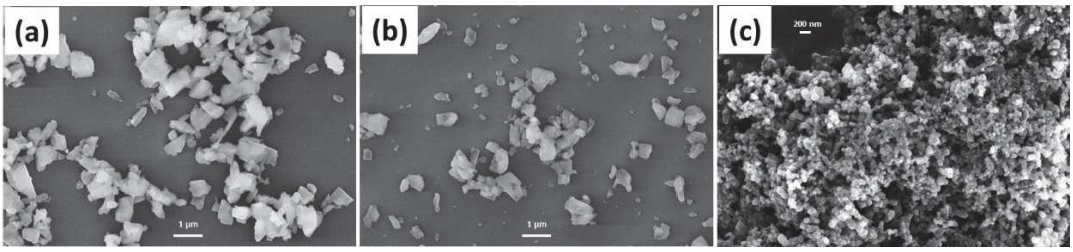

Fig. 2

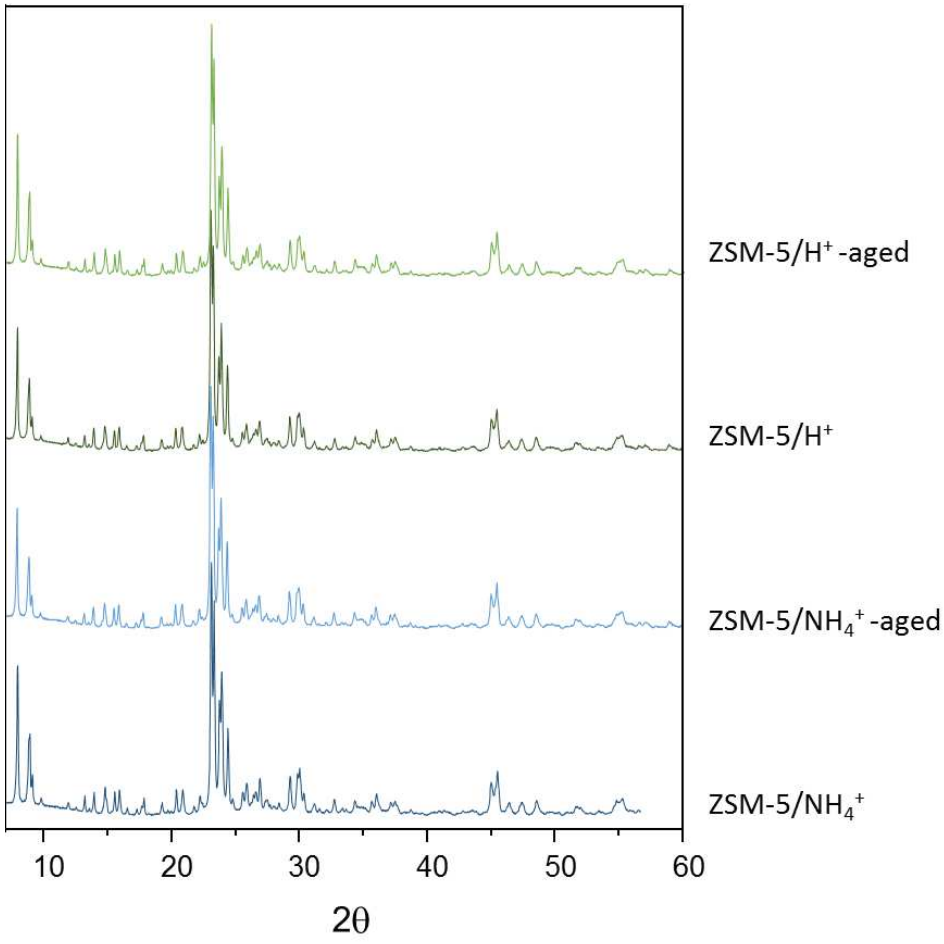

Fig. 3

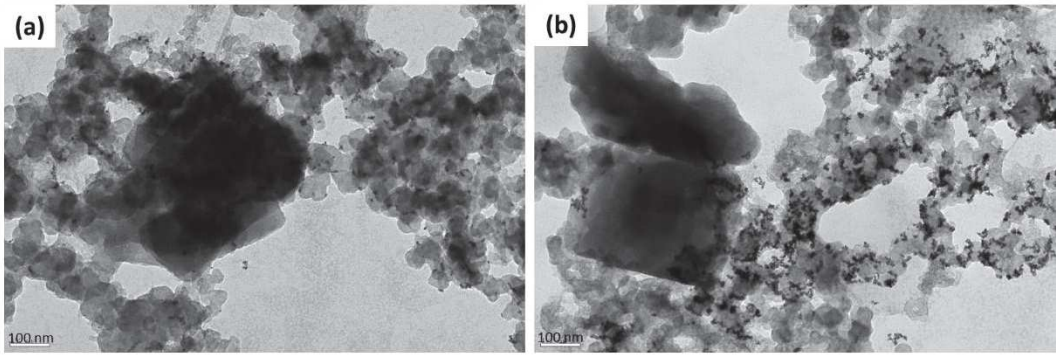

Fig. 4

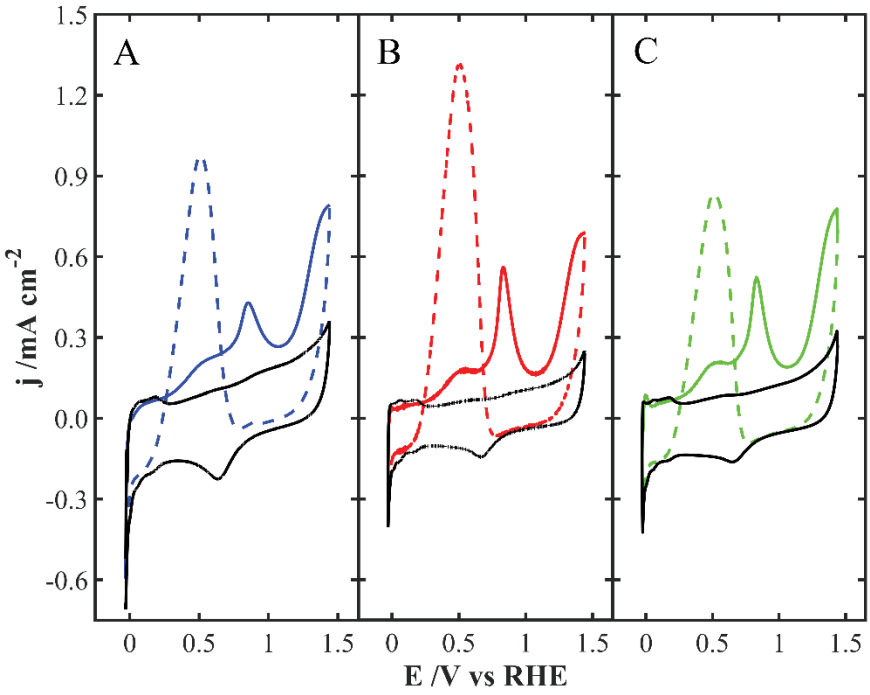

Fig. 5

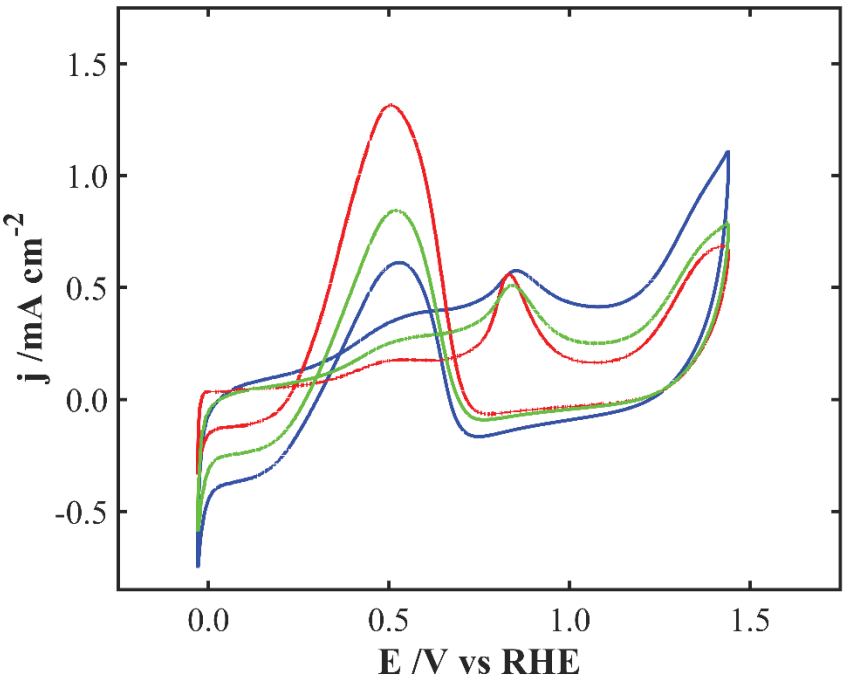

Fig. 6

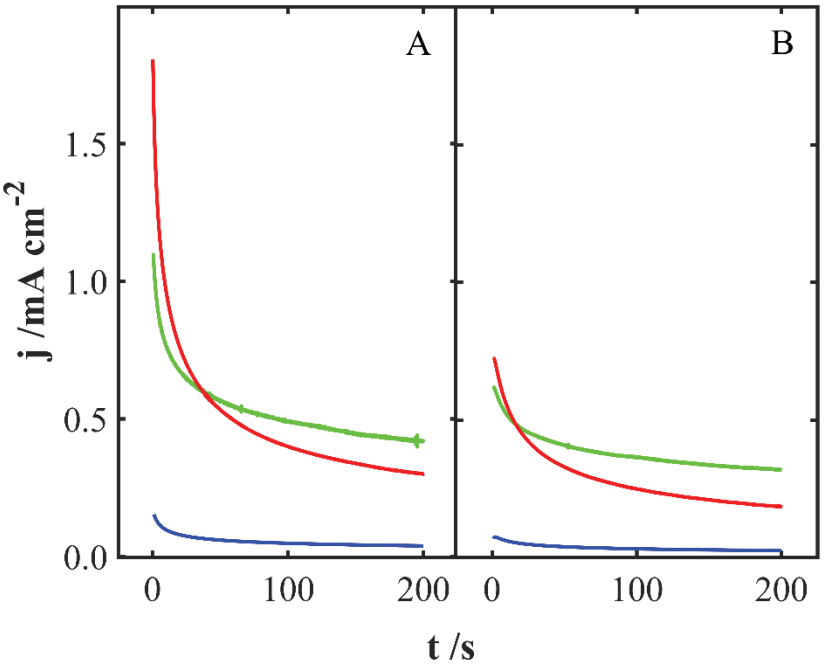

References

[1] J. Qiao, Y. Liu, F. Hong, J. Zhang, Chem. Soc. Rev. 43 (2014) 631–675.

[2] U.O. Nwabara, E.R. Cofell, S. Verma, E. Negro, P.J.A. Kenis, ChemSusChem. 13 (2020) 855–875.

[3] G. Díaz-Sainz, M. Alvarez-Guerra, J. Solla-Gullón, L. García-Cruz, V. Montiel, A. Irabien, J. CO2 Util. 34 (2019) 12–19.

[4] C. Rice, R.I. Ha, R.I. Masel, P. Waszczuk, A. Wieckowski, T. Barnard, J. Power Sources 111 (2002) 83.

[5] C. Rice, S. Ha, R.I. Masel, A. Wieckowski, J. Power Sources 115 (2003) 229.

[6] J.M. Feliu, E. Herrero, in: W. Vielstich, H. Gasteiger, A. Lamm (Eds.) Handbook of Fuel Cells - Fundamentals, Technology and Applications, vol. 2, John Wiley & Sons, Ltd., Chichester, 2003, pp. 625.

[7] P. Strasser, H. Ogasawara, Chemical Bonding at Surfaces and Interfaces. Chapter 6, Surface Electrochemistry, Elsevier, Amsterdam, The Netherlands 2008.

[8] M.T.M. Koper, Fuel Cell Catalysis: A Surface Science Approach, John Wiley & Sons, Hoboken, New Jersey, 2009.

[9] A. Capon, R. Parsons, J. Electroanal. Chem. & Interf. Electrochem. 44 (1973) 1.

[10] A. Capon, R. Parsons, J. Electroanal. Chem. & Interf. Electrochem. 44 (1973) 239.

[11] A. Capon, R. Parsons, J. Electroanal. Chem. & Interf. Electrochem. 45 (1973) 205.

[12] J. Solla-Gullón, V. Montiel, A. Aldaz, J. Clavilier, J. Electroanal. Chem. 491 (2000) 69.

[13] J. Solla-Gullón, F.J. Vidal-Iglesias, A. López-Cudero, E. Garnier, J.M. Feliu, A. Aldaz, Phys. Chem. Chem. Phys. 10 (2008) 3689.

[14] J.V. Perales-Rondón, E. Herrero, J. Solla-Gullón, C.M. Sánchez-Sánchez, J. Electroanal Chem. 793 (2017) 218.

[15] S. Zhang, Y. Shao, H.-G. Liao, J. Liu, I.A. Aksay, G. Yin, Y. Lin, Chem. Mater. 23 (2011) 1079.

[16] S.P.E. Smith, K.F. Ben-Dor, H.D. Abruna, Langmuir 15 (1999) 7325.

[17] A. Boronat-Gonzalez, E. Herrero, J.M. Feliu, J. Solid State Electrochem. 18 (2014) 1181.

[18] J.V. Perales-Rondón, J. Solla-Gullón, E. Herrero, C.M. Sánchez-Sánchez, Appl. Catal., B 201 (2017) 48.

[19] V. Grozovski, V. Climent, E. Herrero, J.M. Feliu, ChemPhysChem 10 (2009) 1922.

[20] V. Grozovski, V. Climent, E. Herrero, J.M. Feliu, Phys. Chem. Chem. Phys. 12 (2010) 8822.

[21] S. Kornic, M. Baker, Chem. Commun. (2002) 1700.

[22] N. Vilà, E. André, R. Ciganda, J. Ruiz, D. Astruc, A. Walcarius, Chem. Mater. 28 (2016) 2511.

[23] F. Yan, M. Wang, Q. Jin, H. Zhou, L. Xie, H. Tang, J. Liu, J. Electroanal. Chem. 881 (2021) 114969.

[24] A. Walcarius, E. Sibbotier, M. Etienne, J. Ghanbaja, Nat. Mater. 6 (2007) 602.

[25] D.R. Rolison, C.A. Bessel, Accounts of Chemical Research 33 (2000) 737.

[26] A. M. Rocco, K. V. Melo, C. J. de A. Mota, M. V. David and I. N. de Souza, Ionics, 25 (2019) 253.

[27] A. Suleiman, C. L. Menéndez, R. Polanco, E. R. Fachini, Y. Hernández-Lebrón, M. J.-F. Guinel, R. Roque-Malherbe and C. R. Cabrera, *RSC Adv.*, 5 (2015) 7637.

[28] A. Medina Ramirez, B. Ruiz Camacho, M. Villicaña Aguilera, I. R. Galindo Esquivel and J. J. Ramírez-Minguela, Appl. Surf. Sci., 456 (2018) 204.

[29] A. Medina Ramírez, M. Villicaña Aguilera, C. M. López-Badillo and B. Ruiz-Camacho, Int. J. Hydrog. Energy, 42 (2017) 30291.

[30] B. M. Daas and S. Ghosh, Electroanalysis, 29 (2017) 2516.

[31] B. M. Daas and S. Ghosh, J. Electroanal. Chem., 783 (2016) 308.

[32] S. Kavian, S. N. Azizi and S. Ghasemi, Int. J. Hydrog. Energy, 41 (2016) 14026.

[33] F. Alidusty, A. Nezamzadeh-Ejhieh, Int. J. Hydrog. Energy, 41 (2016) 6288.

[34] J. Yao and Y. Yao, Int. J. Hydrog. Energy, 41 (2016) 14747.

[35] C. G. Pope, J. Chem. Soc. Faraday Trans., 89 (1993) 1139.

[36] C. G. Pope, J. Chem. Soc. Faraday Trans., 92 (1996) 3647.

[37] T. C. Bowen, L. M. Vane, Langmuir 22 (2006) 3721

[38] H. Zhang, Y. Wang, P. Bai, X. Guo, X. Ni, J. Chem. Eng. Data 61 (2016) 213.

[39] E.E. Mallon, I.J. Babineau, J.I. Kranz, Y. Guefrachi, J.I. Siepmann, A. Bhan, M. Tsapatsis, J. Phys. Chem. B 115 (2011) 11431.

[40] M. León,T.D. Swift, V. Nikolakis, D.G. Vlachos, Langmuir 29 (2013) 6597.

[41] S. Bouden, A. Chaussé, S. Dorbes, O. El Tall, N. Bellakhal, M. Dachraoui, C. Vautrin-Ul, Talanta 106 (2013) 414.

[42] T. Nasir, N.A. Vodolazkaya, G. Herzog, A. Walcarius, Electroanalysis 31 (2019) 202.

[43] S.A. Rezvani, A. Soleymanpour, J. Chromat. A 1436 (2016) 34.

[44] M. Hernandez-Valez, R. Roque-Malherbe, J. Mater. Science Lett. 14 (1995) 1112.

[45] M. Vasić, M. Čebela, I. Pašti, L. Amaral, R. Hercigonja, D. M. F. Santos and B. Šljukić, Electrochim. Acta, 259 (2018) 882.

[46] S. Trasatti, O.A. Petrii, Pure Appl. Chem. 63 (1991) 711.

[47] R. Woods, Chemisorption at electrodes, in: A.J. Bard (Ed.), Electroanalytical Chemistry, 9, Marcel Dekker, New York, 1976.

[48] D. Y. Chung, K.-J. Lee and Y.-E. Sung, J. Phys. Chem. C, 120 (2016) 9028.

[49] F.A. Hanc-Scherer, C.M. Sanchez-Sanchez, P. Ilea, E. Herrero, ACS Catal. 3 (2013) 2935.

[50] J.V. Perales-Rondón, S. Brimaud, J. Solla-Gullón, E. Herrero, R. Jürgen Behm, J.M. Feliu, Electrochim. Acta 180 (2015) 479.

[51] J.V. Perales-Rondon, E. Herrero, J.M. Feliu, Electrochim. Acta 140 (2014) 511.